Journal of Thermal Science and Technology

Vol. 2, No. 2, 2007

Simulation on Soot Oxidation with NO_2 and O_2 in a Diesel Particulate Filter*

Kazuhiro YAMAMOTO**, Shingo SATAKE**, Hiroshi YAMASHITA**,
Akira OBUCHI*** and Junko UCHISAWA***

** Dep. Mechanical Science and Engineering, Nagoya University
Furo-cho, Chikusa-ku, Nagoya, Aichi 464-8603, JAPAN
E-mail: kazuhiro@mech.nagoya-u.ac.jp

*** National Institute of Advanced Industrial Science and Technology (AIST)
16-1 Onogawa, Tsukuba, Ibaraki 305-8569, JAPAN

Abstract

Although diesel engines have an advantage of low fuel consumption in comparison with gasoline engines, exhaust gas has more particulate matters (PM) including soot. As one of the key technologies, a diesel particulate filter (DPF) has been developed to reduce PM. When the exhaust gas passes its porous filter wall, the soot particles are trapped. However, the filter would readily be plugged with particles, and the accumulated particles must be removed to prevent filter clogging and a rise in backpressure, which is called filter regeneration process. In this study, we have simulated the flow in the wall-flow DPF using the lattice Boltzmann method. Filters of different length, porosity, and pore size are used. The soot oxidation for filter regeneration process is considered. Especially, the effect of NO_2 on the soot oxidation is examined. The reaction rate has been determined by previous experimental data. Results show that, the flow along the filter monolith is roughly uniform, and the large pressure drop across the filter wall is observed. The soot oxidation rate becomes ten times larger when NO_2 is added. These are useful information to construct the future regeneration system.

Key words: Porous Media, Catalyst, Combustion Products, Solid Combustion
Diesel Particulate Filter, Diesel Engine, Computational Fluid Dynamics

1. Introduction

Recently, the share of diesel cars in the world is gradually increased, because diesel engines have an advantage of low fuel consumption in comparison with gasoline engines. However, diesel exhaust gas has more ambient air pollutants such as NOx and particulate matters (PM) including soot [(1)(2)]. These emissions are of concern for detrimental effects to human health and the environment, which contribute smog, acid rain, and global warming. Due to the public awareness with regard to harmful emissions, more strict exhaust emissions standards such as Euro V in 2008 are being set in many countries. In Japan, the Tokyo municipal government has begun to regulate diesel-powered vehicles that fail to meet their new emission standards. As one of the key technologies, a diesel particulate filter (DPF) has been developed to reduce PM in the after-treatment of exhaust gas.

In simple explanation of DPF, it traps the soot particles when the exhaust gas passes its porous filter wall. The filtration efficiency is more than 90 %. However, the filter would readily be plugged with particles in a short time. To prevent filter clogging and a rise in backpressure, the accumulated particles must be removed. This is called filter regeneration process. There are two methods, on-board and off-board regenerations. As for the off-board regeneration, the DPF is periodically replaced, or removed to eliminate hydrocarbons and

*Received 31 Jan., 2007 (No. 07-0073)
[DOI: 10.1299/jtst.2.245]

soot by an electric heater. The system is relatively large or complicated, because it is equipped with a temperature controller, compressed air source, and combustion devices.

It is more appropriate to use the on-board regeneration, because it is passive regeneration. That is, the on-board regeneration process is spontaneously conducted during the normal engine operation. To achieve this, oxidation catalysts are used to lower the temperature of soot oxidation [(2)-(7)]. So far, two approaches are known for on-board regeneration. One is to use a Ce-based fuel additive [(8)]. There are two stages for the soot oxidation by Ce. In the first step, the oxidation of Ce_2O_3 by O_2 to produce CeO_2. In the second step, CeO_2 is reacted with soot. However, if the temperature is not sufficient, the presence of additive could prevent the direct soot oxidation by oxygen. Also, it should be rigidly confirmed that the combustion products from Ce are the non-pollutant to the environment.

The other catalytic process we are focusing is the system of soot oxidation by NO_2 [(4),(9)-(11)], which promotes soot oxidation indirectly. Catalytic reactions with Pt oxidize NO in exhaust gas into NO_2, which reacts with soot to produce CO and CO_2. Different from Ce-based fuel additive, NO and NO_2 naturally exist in exhaust gas. It should be emphasized that NO_2 is much more reactive than O_2. However, the reaction rate and quantitative effect of NO_2 on soot oxidation is not clear, especially in the DPF system. In this paper, using the lattice Boltzmann method (LBM), we simulate the soot combustion for the filter regeneration process. The reaction rate is estimated from previous experimental data for model soot oxidation with NO_2.

2. Numerical Method

The filter is mostly made of cordierite or SiC to have complex inner structure with small pore (typically less than 10 microns) [(12)]. So far, it is difficult to observe the phenomena inside the filter experimentally. We can not insert the probe or hot film sensor for flow measurement inside the ceramic wall. Since the cell size of DPF is small and is not transparent, we can not use a laser technique such as LDV or PIV, either. Magnetic Resonance Imaging (MRI) may be applied, but the time resolution is not enough to measure the high velocity such as exhaust gases. Additionally, we don't have enough information on the particle trap or filter regeneration process. Although numerical simulation is the only way to investigate the phenomena in DPF, it is very challenging to deal with this process by conventional CFD code, because we need to consider the small scale and complex geometry with chemical reaction. Then, we have focused on the lattice Boltzmann method (LBM).

The fundamental idea of LBM is to construct simplified kinetic models that incorporate the essential physics of microscopic or mesoscopic processes so that the macroscopic averaged properties obey the desired macroscopic equations such as the N-S equation. The kinetic equation provides any of the advantages of molecular dynamics, including clear physical pictures and fully parallel algorisms [(13)]. The LBM fulfills these requirements in a straightforward manner, and the treatment of boundary conditions is simple and easy, and it is appropriate to calculate porous media flow [(14)-(18)]. Recently, we have conducted the combustion simulation in three-dimensional porous structure by LBM [(19)].

Here, we explain the numerical procedure in combustion simulation [(19)-(21)]. The flow is described by the lattice BGK equation in terms of the distribution function. For three-dimensional simulation, D3Q15 model [(16)] evolves on the lattice space with 15 discrete velocities in Fig. 1. The following 15 unit velocity vectors are shown in Eq. 1.

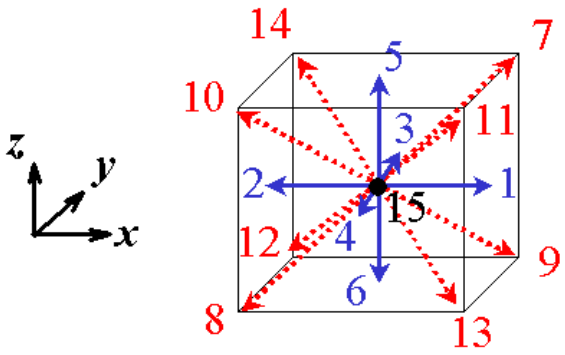

Figure 1 D3Q15 model for 3D simulation.

$$\begin{bmatrix} \boldsymbol{c}_1 & \boldsymbol{c}_2 & \boldsymbol{c}_3 & \boldsymbol{c}_4 & \boldsymbol{c}_5 & \boldsymbol{c}_6 & \boldsymbol{c}_7 & \boldsymbol{c}_8 & \boldsymbol{c}_9 & \boldsymbol{c}_{10} & \boldsymbol{c}_{11} & \boldsymbol{c}_{12} & \boldsymbol{c}_{13} & \boldsymbol{c}_{14} & \boldsymbol{c}_{15} \end{bmatrix}$$
$$= c \begin{bmatrix} 1 & -1 & 0 & 0 & 0 & 0 & 1 & -1 & 1 & -1 & 1 & -1 & 1 & -1 & 0 \\ 0 & 0 & 1 & -1 & 0 & 0 & 1 & -1 & 1 & -1 & -1 & 1 & -1 & 1 & 0 \\ 0 & 0 & 0 & 0 & 1 & -1 & 1 & -1 & -1 & 1 & 1 & -1 & -1 & 1 & 0 \end{bmatrix} \quad (1)$$

To reduce the calculation time, D2Q9 model for 2D simulation is also used to consider the real size of DPF. The evolution equation using the pressure distribution function is,

$$p_\alpha(\boldsymbol{x} + \boldsymbol{c}_\alpha \delta_t,\ t + \delta_t) - p_\alpha(\boldsymbol{x},\ t) = -\frac{1}{\tau}[p_\alpha(\boldsymbol{x},\ t) - p_\alpha^{eq}(\boldsymbol{x},\ t)] \quad (2)$$

where δ_t is the time step, and τ is the relaxation time that controls the rate of approach to equilibrium. The equilibrium distribution function, p_α^{eq}, is given by

$$p_\alpha^{eq} = w_\alpha \left\{ p + p_0 \left[3\frac{(\boldsymbol{c}_\alpha \cdot \boldsymbol{u})}{c^2} + \frac{9}{2}\frac{(\boldsymbol{c}_\alpha \cdot \boldsymbol{u})^2}{c^4} - \frac{3}{2}\frac{\boldsymbol{u} \cdot \boldsymbol{u}}{c^2} \right] \right\} \quad (3)$$

where w_α = 1/9 (α = 1 to 6), w_α = 1/72 (α = 7 to 14), and w_{15} = 2/9. The sound speed, c_s, is $c/\sqrt{3}$ with $p_0 = \rho_0 R T_0 = \rho_0 c_s^2$. Here, p_0 and ρ_0 are the pressure and density at the room temperature, T_0. The pressure and local velocity of $\boldsymbol{u}=(u_x, u_y, u_z)$ are obtained by Eqs. 4 and 5, which is based on the low Mach number approximation [22]. The velocity is accelerated due to heat expansion by soot oxidation (combustion).

$$p = \sum_\alpha p_\alpha \quad (4)$$

$$\boldsymbol{u} = \frac{\rho_0}{\rho}\frac{1}{p_0}\sum_\alpha \boldsymbol{c}_\alpha p_\alpha \quad (5)$$

The relaxation time is related with transport coefficients, such as kinetic viscosity and diffusion coefficient using $\nu = (2\tau - 1)/6\, c^2 \delta_t$. Through the Chapman-Enskog procedure, the Navier-Stokes equations are derived from these equations [13].

The LBM formula for temperature and concentration fields is,

$$F_{s,\alpha}(\boldsymbol{x}+\boldsymbol{c}_\alpha\delta_t,\ t+\delta_t) - F_{s,\alpha}(\boldsymbol{x},\ t) = -\frac{1}{\tau_s}[F_{s,\alpha}(\boldsymbol{x},\ t) - F_{s,\alpha}^{eq}(\boldsymbol{x},\ t)] + w_\alpha Q_s, \quad s = T,\ Y_i \quad (6)$$

where Q_s, is the source term due to chemical reaction, which is described by the Arrhenius-type reaction. The experimental procedure to determine the reaction rate is explained later. The temperature, T, and mass fraction of species, Y_i, are determined by these distribution functions.

$$T = \sum_{\alpha} F_{T,\alpha} \qquad (7)$$

$$Y_i = \sum_{\alpha} F_{Yi,\alpha} \qquad (8)$$

Figure 2 shows the schematics of DPF system. This wall-flow filter is designed with a honeycomb structure with adjacent air holes closed at alternate ends so that the flow passes through the porous wall. Two types of calculation domain are adopted. Domain 1 is of 140 mm × 2 mm for the simulation of regeneration process. The total number of grids is 4201 (N_x)×61 (N_y), with grid size of 0.03 mm. The monolith length of the cell is L, and the wall thickness is W. The properties of the filters are shown in Table 1. The cell concentration is 200 cells/in^2. To change the porosity, e, and the mean pore size, d, we form the porous structure by simulation [23][24]. The porosity and pore size are freely selected. The pore size in this calculation is 9 or 33 μm, which is the typical value of SiC and cordierite filters [12], respectively. Domain 2 is used for the particle trap simulation. To predict the filter backpressure more precisely, the three-dimensional simulation is needed. This is because the friction factor in the porous media flow is unrealistically higher if the flow normal to x-y plane is not considered [25]. Domain 2 is of 0.16 mm × 0.80 mm × 0.16 mm. The total number of grids is 41 (N_x)×201 (N_y)×41 (N_z), with grid size of 0.004 mm. The inflow velocity, U_0, is 10 cm/s and 100 cm/s.

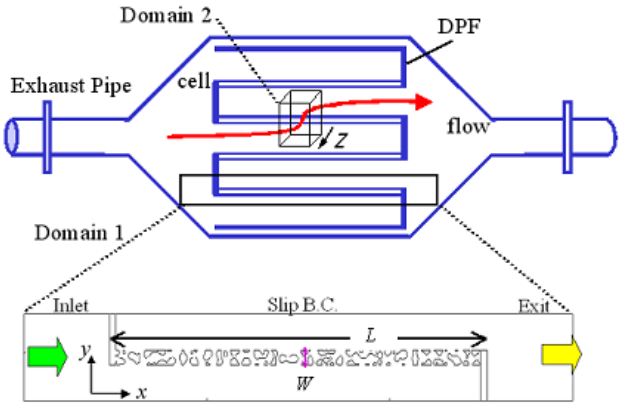

Figure 2 Schematics of DPF system and calculation domain with coordinate.

Table 1 Properties of DPF in this study.

Property	Scale
Length, L (mm)	13, 133
Cell size (mm)	1.5×1.5 (200 cells/in^2)
Wall Thickness, W (mm)	0.4
Porosity, e (%)	42, 60, 75
Mean pore size, d (μm)	33, 9

As for the boundary condition, the inflow boundary is adopted at the inlet [26]. The mixture corresponds to the diesel exhaust gas with 10 % O_2. Its temperature is set to be 900 K. At the sidewall, the slip boundary conditions are adopted, considering the symmetry [17]. At the outlet, the pressure is constant, and the gradient of scalar such as temperature and mass fraction is set to be zero. On the surface of the obstacle, the so-called bounce-back rule for non-slip wall is adopted [19][20]. Since there is no accurate data for soot oxidation with NO_2, the activation energy and the pre-exponential factor needed in the simulation are estimated by previous experiments [4].

3. Results and Discussion

3.1 Experiments for Soot Oxidation

First, the rate of soot oxidation is estimated by previous experiments[4]. Temperature-programmed reactions (TPR) were carried out to evaluate the catalytic performance for soot oxidation. Commercially available carbon black (CB; Nippon Tokai carbon 7350F; primary particle size = 28 nm; specific surface area = 80 m^2/g) was used as model soot. The mixture of SiO_2 (0.5 g) and CB powder (0.005 g) were placed in the reactor. For the regeneration process with NO_2, 1000 ppm NO_2 was added in the flow. Other gases included were 7% H_2O, 10% O_2 and N_2, corresponding to the composition of diesel exhaust gas. The concentration of CO, CO_2, NO, and temperature, T, were monitored.

Figure 3 shows the test results for CB oxidation in the flow with NO_2. When CB is reacted with NO_2 as well as O_2, CO and CO_2 are produced. From this figure, it is found that the oxidation is initiated at 720 K and peak temperature for maximum oxidation rate is achieved at the temperature of 850 K. On the other hand, in the experiments without NO_2, TPR profile was much different. In this case, the oxidation is initiated at 760 K and peak temperature for maximum oxidation rate is around 940 K. Then, the oxidation of CB is much promoted by adding NO_2.

Next, we estimate the reaction rate of soot oxidation. Since there is enough oxygen burning off (oxidizing) the CB, it is assumed that the reaction rate is expressed by the reaction rate constant, k_r, and the mass of CB, M_{CB}.

$$-\frac{dM_{CB}}{dt} = k_r M_{CB} \quad (9)$$

The equation for $\ln(k_r)$ can be derived from the natural logarithm of the Arrhenius equation.

$$\ln(k_r) = \ln A - \frac{E}{RT} \quad (10)$$

As seen in Fig. 3, NO is produced by the reaction of NO_2 with soot. Although it has been confirmed that, when $T > 650$ K, the concentration of NO_2 is in equilibrium values between NO and NO_2 when the Pt catalyst is present [4], the oxidation rate of CB could be varied when the concentration of NO_2 is largely changed. Therefore, we estimate the reaction constants of Arrhenius factor, A, and activation energy, E, in the temperature range of 670 K to 770 K. Figure 4 shows Arrhenius plotting with and without NO_2. The estimated values of Arrhenius factor and activation energy are as follows:

With NO_2: A = 146 1/s, E = 79.5 kJ/mol (11)

Without NO_2: A = 1.20 1/s, E = 64.9 kJ/mol (12)

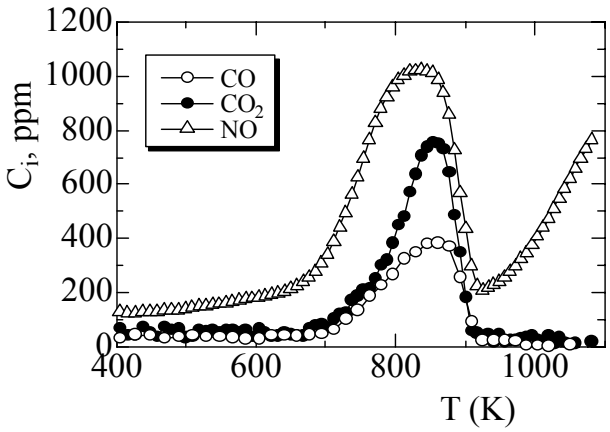

Figure 3 Concentration of products at temperature programmed reactions (TPR) in 1000 ppm NO_2 + 7% H_2O + 10% O_2 in N_2.

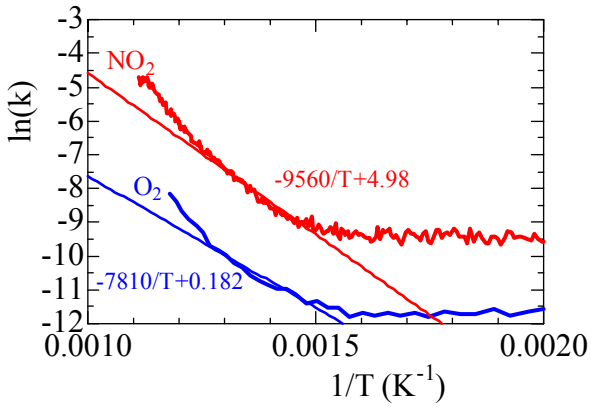

Figure 4 Arrhenius plotting at temperature programmed reactions (TPR) with and without NO_2.

3.2 Flow in DPF

First, we examine the flow field in DPF. In measurements, only filter backpressure and velocity profiles downstream from the DPF exit can be measured [12][25]. There is little information on the velocity inside the filter. Numerical simulation is the only way to investigate the flow field directly. Figure 5 shows the velocity field in DPF. Its porosity is 0.6, and the pore size is 33μm. The monolith length is 13mm. The distributions of velocity vector, mass flux in the *x*-direction, and pressure are shown. Since the exit of the monolith is closed and the flow passes through the porous wall, the mass flux is gradually decreased. The velocity profile passing through the wall will be discussed later. At the opposite side of the wall, the flow rate is again increased toward the exit. As seen in the pressure distribution, the pressure gradually decreases along the flow path, but there is a huge pressure drop across the filter wall.

Next, the velocity passing through the filter wall is examined. Since the soot particles in exhaust gas are transported by the flow, the particle accumulation is largely affected by the distributions of velocity in *x*-direction (along the monolith). To check the profile using different monolith length, we use two filters of L = 13 and 133 mm. To maintain the mean flow velocity across the wall, the inflow velocity, U_0, is 10 cm/s and 100 cm/s, respectively.

The porosity and pore size is the same in Fig. 5. Results are shown in Fig. 6. The velocity is smaller than the inflow velocity, because the monolith length is larger than the inlet width (cell width). In some area, the velocity is almost zero. This is because the flow passes only through the pore inside the wall and there are some paths with no exits. It is interesting to note that, independent of the monolith length, the velocity profile is almost uniform along the x-direction.

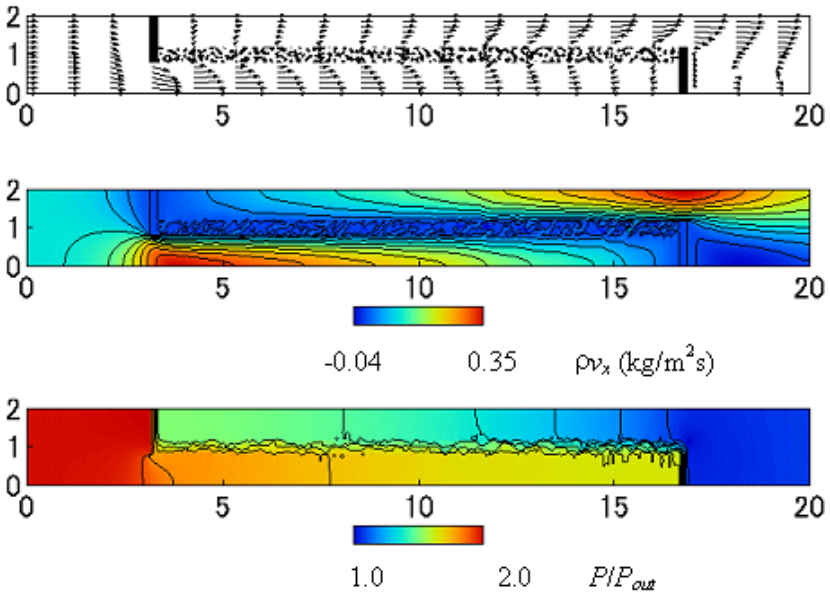

Figure 5 Velocity field in DPF for $e = 0.6$, $L = 13$mm, $d = 33$ μm, $U_0 = 10$ cm/s; velocity vector, mass flux in x-direction, and pressure distributions are shown.

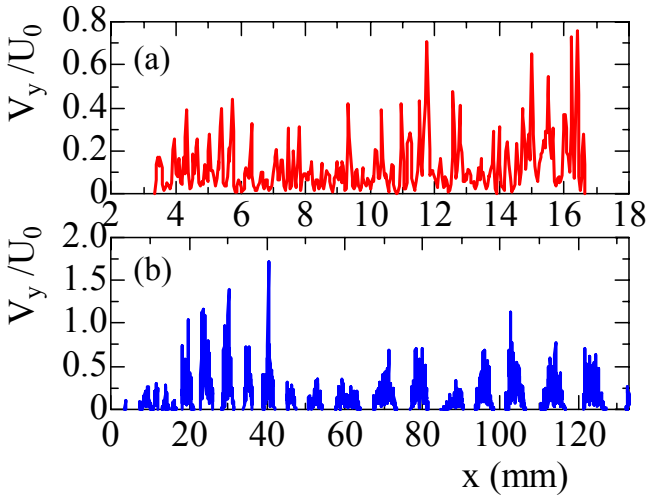

Figure 6 Profiles of velocity passing through porous wall for $e = 0.6$, $d = 33$ μm; (a) $L = 13$ mm, $U_0 = 10$ cm/s, (b) $L = 133$ mm, $U_0 = 100$ cm/s.

In order to avoid plugging the filter with diesel particles, we usually monitor the backpressure, which depends on the flow velocity, the degree of the trapped particles, and the inner structure of the diesel filter [12]. As seen in Fig. 6, the velocity profile is roughly

uniform along the monolith (x-direction in Fig. 2). Also, the backpressure corresponds to the pressure drop across the filter wall. Here, to compare the experimental results using the real filter, three-dimensional simulation is conducted in Domain 2. Calculated pressure profiles are shown in Fig. 7. The inflow velocity is 100 cm/s, and the filter wall is located at y = 0.2 to 0.6 mm. The porosities considered are 0.42, 0.6, and 0.75. The mean pore size is 9 μm of the typical value of SiC DPF.

The pressure is averaged in x-z plane. The pressure starts to decrease almost linearly, although it slightly fluctuates for e = 0.42. This could be due to the spatial non-uniformity of porosity. After passing this region, the pressure is constant. To compare three cases, it is found that, as the porosity is smaller, the pressure at the inlet is larger. According to the following Darcy's law,

$$u = -\frac{k}{\mu}\nabla p \quad (13)$$

where, k is the permeability, μ is the viscosity, and ∇p is the pressure gradient in the flow direction of u. The estimated permeability from this figure is 3.5 $\times 10^{-13}$ m^2 for e = 0.42, 5.6 $\times 10^{-13}$ m^2 for e = 0.60, and 6.3 $\times 10^{-13}$ m^2 for e = 0.75. Since the reported value of SiC DPF for e = 0.42 [12] is 3.7 $\times 10^{-13}$ m^2, it is confirmed that the porous structure formed by our simulation is similar to the real SiC DPF.

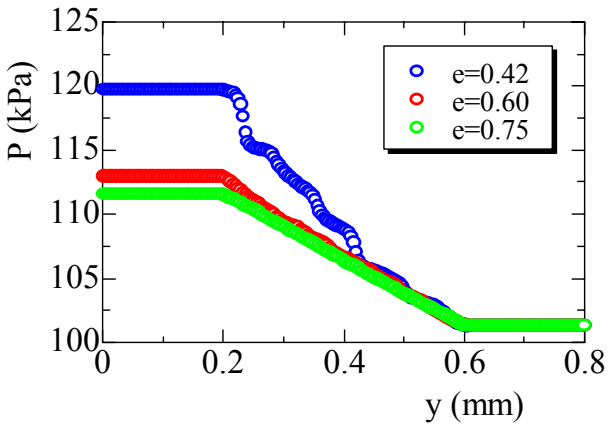

Figure 7 Pressure distributions across filter wall for e = 0.42, 0.6, and 0.75; W = 0.4 mm, d = 9 μm, U_0 = 100 cm/s.

3.3 Soot Oxidation for Filter Regeneration Process

Finally, the soot oxidation is simulated for the filter regeneration process. It is assumed that the soot is homogeneously attached to the filter wall surface. Since the reaction rate estimated by experiments is used, the catalytic effect in the reaction is already included. The mass of soot on the filter wall surface is 3×10^{-10} g/grid, corresponding to 0.37 g/L based on the unit volume of DPF. The oxygen concentration is 10% in the inflow gas, which is the same value in the experiment [4]. Since exhaust gas temperature is 900 K, the soot is reacted with oxygen. Time, t, is counted after we start the simulation. Figure 8 shows the distributions of velocity vector, temperature, mass of soot, and the reaction rate at t = 100 ms. These are obtained with the reaction in the flow with NO_2 addition. The porosity is 0.6 and the pore size is 33 μm. The velocity is accelerated due to the temperature increase. Since the soot on the filter surface is burned, the maximum temperature is higher than the exhaust gas temperature. Roughly, one-third of the soot is already burned.

To evaluate the effect of NO_2 on the soot oxidation, the combustion simulation is

conducted using the two reaction rates with and without NO_2. Figure 9 shows the maximum temperature and mass of remained soot in DPF. As seen in Fig. 9(a), the temperature rise occurs earlier under NO_2 coexistence. According to Setiabudi et al. [11], the surface oxygen complexes is formed as soot oxygen intermediates, and a higher oxygen rate is observed in NO_2 - soot reaction. In our simulation, it is estimated that the soot oxidation rate becomes ten times larger in the presence of NO_2. That is, the soot reaction is largely accelerated with NO_2 addition, and the effectiveness of regeneration process by NO_2 is confirmed in wall-flow DPF system.

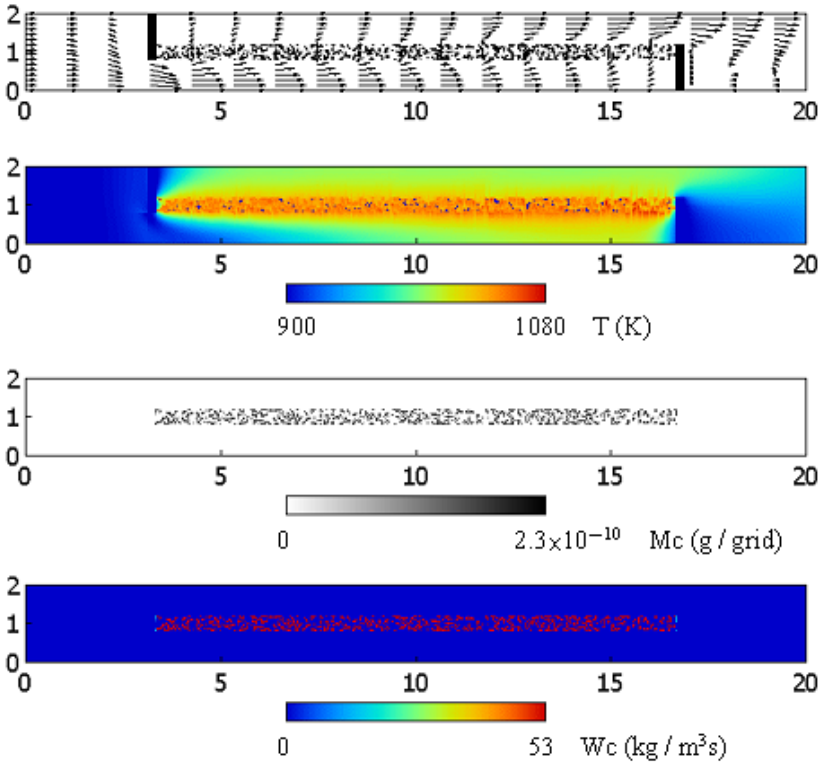

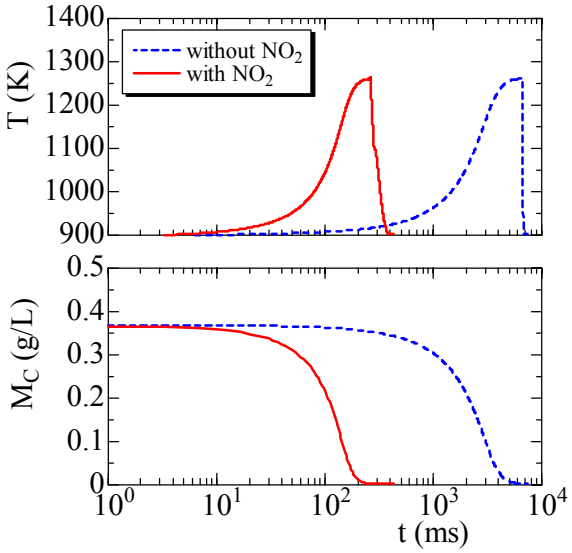

Figure 9 Maximum temperature and mass of remained soot in DPF for $e = 0.6$, $L = 13$mm, $d = 33$ μm, $U_0 = 10$ cm/s to observe effect of NO_2 on soot oxidation.

4. Conclusions

We have simulated the flow in a wall-flow DPF using the lattice Boltzmann method. Filters of different length, porosity, and pore size are used. The soot oxidation for filter regeneration process is considered. Especially, the effect of NO_2 on the soot oxidation is examined, which was recently proposed as the on-board regeneration system. The reaction rate has been determined by the previous experimental data. The estimated values of Arrhenius factor and activation energy are A = 146 1/s, E = 79.5 kJ/mol with NO_2, and A = 1.20 1/s, E = 64.9 kJ/mol without NO_2.

Results show that, the flow along the filter monolith is roughly uniform, and the large pressure drop across the filter wall is observed, corresponding to the filter backpressure. The obtained permeability based on the Darcy's law is close to the reported value of SiC DPF. When the porosity of the filter is reduced, the filter backpressure is largely increased. In soot oxidation process, the soot oxidation rate becomes ten times larger when NO_2 is added. These are useful information to construct the prediction model for after-treatment of soot particles in exhaust gas, and to develop the future regeneration system.

Acknowledgements

This work was partially supported by New Energy and Industrial Technology Development Organization (Industrial Technology Research Grant, 05A18020d) and The Hibi Science Foundation in Japan.

References

(1) J. C. Clerc, Catalytic diesel exhaust aftertreatment, Applied Catal. B 10(1996) 99-115.
(2) H. J. Stein, Diesel oxidation catalysts for commercial vehicle engines: stratefies on their application for controlling particulate emissions, Appl. Catal. B 10 (1996) 69-82.
(3) G. Neri, L. Bonaccorsi, A. Donato, C. Milone, M. Grazia, A.M. Visco, Catalytic combustion of diesel soot over metal oxide catalysts, Appl. Catal. B 11 (1997) 217-231.
(4) J. Oi-Uchisawa, A. Obuchi, A. Ogata, R. Enomoto, and S. Kushiyama, Effect of feed gas composition on the rate of carbon oxidation with Pt/SiO_2 and the oxidation mechanism, Applied Catal. B 21(1999) 9-17.
(5) B. Dernaika, D. Uner, A simplified approach to determine the activation energies of uncatalyzed and catalyzed combustion of soot, Appl. Catal. B 40 (2003) 219-229.
(6) S. Wang and B. S. Haynes, Catalytic Combustion of soot on metal oxides and their supported metal chlorides, Catalysis Communications 4 (2003) 591-596.
(7) R. López-Fonseca, U. Elizundia, I. Landa, M. A. Gutiérrez-Ortiz, J. R. González-Velasco, Kinetic analysis of non-catalytic Mn-catalysed combustion of diesel soot surrogates, Appl. Catal. B 61 (2005) 150-158.
(8) G. C. Koltsakis and A. M. Stamatelos, Modeling thermal regeneration of wall-flow diesel particulate traps, AIChE J., 42(6) (1996) 1662-1672.
(9) B. J. Cooper, H. J. Jung, and J. E. Toss, US Patent, 4902487(1990).
(10) P. Hawker, Diesel emission control technology, Platinum Metals Rev. 39 (1995) 2-8.
(11) A. Setiabudi, M. Makkee, J. A. Moulijn, The role of NO_2 and O_2 in the accelerated combustion of soot in diesel exhaust gases, Appl. Catal. B 50 (2004) 185-194.
(12) G. A. Stratakis and A. M. Stamatelos, Flow maldistribution measurements in wall-flow diesel filters, Proc. Instn. Mech. Engrs., Vol. 218, Part D (2004) 995-1009.
(13) S. Chen, and G. D. Doolen, Lattice Boltzmann method for fluid flows, Annual Reviews of Fluid Mech. Vol.30 (1998) 329-364.
(14) G. McNamara and G. Zanetti, Use of the Boltzmann equation to simulate lattice-gas automata, Phys. Review Lett., **61** (1988) 2332-2335.

(15) A. Cancelliere, C. Chang, E. Foti, D.H. Rothman and S. Succi, The permeability of a random medium: comparison of simulation with theory, Phys. Fluids A, **2** (1990) 2085-2088.
(16) Y. H. Qian, D. d'Humie`res and P. Lallemand, Lattice BGK models for Navier-Stokes equation, Europhys. Lett., **17** (1992) 479-484.
(17) T. Inamuro, M. Yoshino, and F. Ogino, Lattice Boltzmann simulation of flows in a three-dimensional porous structure, Int. J. Numer. Methods Fluids 29 (1999), 737-748.
(18) J. Bernsdorf, G. Brenner, and F. Durst, Numerical analysis of the pressure drop in porous media flow with lattice Boltzmann automata, Comput. Phys. Commun. 129 (2000) 247-255.
(19) K. Yamamoto, N. Takada, and M. Misawa, Combustion Simulation with Lattice Boltzmann Method in a Three-Dimensional Porous Structure, Proc. Comb. Inst. **30** (2005) 1509-1515.
(20) K. Yamamoto, X. He, and G. D. Doolen, Simulation of Combustion Field with Lattice Boltzmann Method, J. Statistical Physics, Vol. 7, Nos.1/2 (2002) 367-383.
(21) K. Yamamoto, X. He, and G. D. Doolen, Combustion Simulation using the Lattice Boltzmann Method, JSME Int. J., Series B, Vol.47, No.2 (2004), 403-409.
(22) O. Filippova D. and Hänel, Computer Physics Communications, 129 (2000) 267-274.
(23) K. Yamamoto and N. Takada, LB Simulation on Soot Combustion in Porous Media, Physica A 362 (2006), 111-117.
(24) K. Yamamoto, S. Satake, H. Yamashita, N. Takada, and M. Misawa, Lattice Boltzmann Simulation on Porous Structure and Soot Accumulation, Math. Computers in Simulation 72 (2006) 257-263.
(25) R. B. Bird, W. E. Stewart and E.N. Lightfoot, Transport Phenomena, Wiley, New York (1960).
(26) X. He, S. Chen, and G. D. Doolen, A Novel Thermal Model for the Lattice Boltzmann Method in Incompressible Limit, J. Comput. Phys. 146 (1998) 282-300.